


# Fuzzy Scheduled Optimal Control of Integrated Vehicle Braking and Steering Systems

Mehdi Mirzaei  and Hossein Mirzaeinejad

**Abstract**—The safe hard braking of a turned vehicle requires short stopping distance while maintaining the vehicle in the path. To achieve the first aim, a wheel slip controller is designed to calculate the maximum braking force of each wheel according to the tire/road conditions. For the second aim, a new optimal multivariable controller for integrated active front steering and direct yaw moment control is analytically developed to control the vehicle directional stability directly. Since the required stabilizing external yaw moment has to be produced by reducing the maximum achievable braking forces of one side wheels, it leads to increase the stopping distance and should be kept as low as possible. In an effective way to manage the integrated control inputs, a fuzzy logic is defined to determine the weight factor of each control input in the integrated optimal control law. This logic is defined using the stability index obtained by the phase plane analysis of nonlinear vehicle model. Therefore, the proposed controller can be tuned automatically for different driving conditions. The simulation results carried out using a validated vehicle model demonstrate that the integrated control system has a better performance compared with stand-alone braking and steering systems to attain the desired purposes.

**Index Terms**—Directional stability, fuzzy scheduling, integrated braking and steering, optimal nonlinear control, stopping distance, vehicle control.

## I. INTRODUCTION

CHASSIS control systems have been popular research topics to enhance the vehicle dynamic behavior under critical driving situations. Among these systems, the antilock braking system (ABS), the active front steering (AFS), and the electronic stability program (ESP) have been frequently employed to improve the vehicle active safety performance.

ABS is a well-known active safety system regulating the wheel longitudinal slip to generate the maximum braking force.

Manuscript received April 7, 2016; revised September 14, 2016, January 2, 2017, March 7, 2017, and June 29, 2017; accepted August 27, 2017. Date of publication September 3, 2017; date of current version October 13, 2017. Recommended by Technical Editor J. C. Koo. (Corresponding author: Mehdi Mirzaei.)

M. Mirzaei is with the Department of Mechanical Engineering, Sahand University of Technology, Tabriz 51335-1996, Iran (e-mail: mirzaei@sut.ac.ir).

H. Mirzaeinejad is with the Department of Mechanical Engineering, Shahid Bahonar University of Kerman, Kerman 68366-71111, Iran (e-mail: h\_mirzaeinejad@uk.ac.ir).

Color versions of one or more of the figures in this paper are available online at <http://ieeexplore.ieee.org>.

Digital Object Identifier 10.1109/TMECH.2017.2749002

In several studies, the conventional ABS is designed for vehicles traveling along a straight line, where only the longitudinal dynamics is interfered [1]–[3]. However, the hard braking during turning or on the asymmetric road surface such as the split- $\mu$  road causes an undesirable vehicle yaw moment [4], [5]. This unexpected yaw moment may result the loss of vehicle directional stability. Therefore, during hard braking while turning, maintaining the vehicle stability and steerability are as important as attaining short stopping distance. In this situation, the conventional ABS cannot maintain the vehicle directional stability completely and its integration with other chassis control systems is required.

A common system for the direct control of vehicle steerability is AFS in which the front steering angle is controlled to affect on the tire lateral forces [6], [7]. The main problem of active steering system is its limitation due to the inherent saturation property of tire lateral force [7]. When the tire lateral force is near saturation, its direct effectiveness from the steer input is lost [7], [8]. In order to compensate the limitation of steering control system especially in nonlinear regimes of vehicle dynamics, the ESP technology has been introduced to generate a corrective stabilizing yaw moment by applying different longitudinal forces between the left and right tires [7]–[9]. By this technology, the vehicle directional stability is provided by limiting the side slip angle in an admissible range. For the application of ESP, hardware components of the ABS are used and, therefore, additional actuator is not required in contrast to active rear-wheel steering system [10]. However, the main deficiency of ESP addressed by researchers, is providing undesirable driving conditions due to the intentional changes in braking forces [5], [11]. One of the recent approaches to limit the excessive use of external yaw moment is to integrate the ESP with AFS [11], [12]. By this approach, the external yaw moment is only generated to compensate the limitation of steering control.

Different control strategies have been presented for the integrated control of AFS and ESP systems in the literature. An integration of AFS and direct yaw moment control (DYC) was proposed based on the optimal guaranteed cost control technique [11]. Boada *et al.* [12] designed a control system by integrating the front wheel steering control and front braking force distribution using fuzzy logic control. In [13], the feedback linearization technique was applied to integrate the braking and steering subsystems. A multivariable nonlinear optimal controller was proposed based on the state-dependent Riccati equation technique to stabilize the vehicle dynamics using individual braking torque and steering angle [14]. In [15], a vehicle yaw

stabilization scheme was presented based on the dynamic control allocation method using braking and steering actuators. Hwang *et al.* [16] investigated the integrated control of AFS and ESP by using a frequency domain multivariable control technique. In another work, the coordination of AFS and differential braking was presented by applying the model predictive control strategy [17].

In most studies reviewed above, the ESP system is utilized to improve the maneuverability of vehicle which turns with high speeds on various road conditions. In this case, the minimum usage of intentional asymmetric braking force for the small reduction of vehicle velocity is desired. However, the hard braking of a turned vehicle is another scenario in which the short stopping distance while maintaining the vehicle directional stability should be provided. In this case, the maximum braking forces of one side wheels achievable by the conventional ABS are released to generate the required external stabilizing yaw moment. This intentional reduction of maximum braking force leads to a long stopping distance and should be kept as low as possible. In this respect, recent findings were reported by Mirzaeinejad and Mirzaei [5] with the simulation studies for the hard braking on a split- $\mu$  road. In the mentioned work, only the braking system is controlled by an optimal algorithm to achieve the shortest stopping distance at the cost of some deviations from the straight line.

In the present study, the combined braking and steering systems are controlled in an optimal way for a steered vehicle under hard braking. This is a new scenario for which the enhanced braking performance with the improvement of lateral stability is desired. In this way and in order to achieve the directional stability with a small reduction of maximum braking force achievable by the conventional ABS, the AFS is optimally integrated with the braking control system. Therefore, the shortest stopping distance while maintaining the directional stability can be achieved. Here, a new multivariable controller is optimally designed for the integrated AFS and DYC based on the prediction of nonlinear responses of a validated eight degrees of freedom (8-DOF) vehicle model. By this method, the effects of normal load transfer have been considered in the controller design. The performance index including the weighted combination of two control inputs and the next tracking errors of vehicle yaw rate are minimized to analytically develop the multivariable control law in the closed form. The controller performance is analytically evaluated and the error analysis in the presence of modeling uncertainties is presented. In an effective idea, the weight factors, as the free parameters of the integrated control laws, are online regulated based on fuzzy logics to determine the effective contribution of each control input at each time. The input of fuzzy system is the stability index obtained from the phase plane analysis of the nonlinear vehicle model. With the proposed fuzzy scheduled method, the designed integrated controller is tuned automatically and the weight factors are changing softly for different driving conditions. By determination of the weight factors in limit conditions, the integrated control law easily leads to the stand-alone braking and steering control laws. A gain scheduling type of linear optimal regulator was proposed in [18]

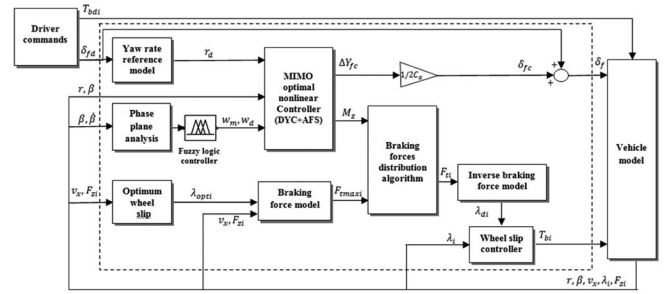


Fig. 1. Overall structure of the proposed integrated control system.

to attenuate the roll due to the waves for a monohull ship. In this paper, a neural network was adopted to interpolate the suitable gains for the controller at any time from estimation of the sea conditions.

The proposed integrated control system provides the possibility of calculating the stabilizing external yaw moment as low as possible. Therefore, a small reduction of the maximum braking forces is required, which leads to the shortening stopping distance. At the rest of the paper, an optimal nonlinear algorithm for the proper distribution of tire braking forces is also presented. In this algorithm, the maximum braking force of one side wheels, achievable by the conventional ABS, is reduced to the extent that the required external yaw moment can be produced. At the end of this paper, simulation studies have been performed using validated vehicle models to evaluate the performance and robustness of the proposed integrated control system.

## II. STRUCTURE OF THE PROPOSED CONTROL SYSTEM

The structure of the proposed control system is shown in Fig. 1.

For a fast stopping during turning, the driver applies the steering angle  $\delta_{fd}$  and the hard braking torques  $T_{bdi}$ . These two driver commands are modified or changed by the control system. First, according to the reference yaw rate corresponding to the driver steering angle, a multivariable optimal nonlinear controller is designed to compute the required yaw moment and the corrective lateral force of the front wheels ( $M_z, \Delta Y_{fc}$ ). Also, the controller weight factors ( $w_m, w_d$ ) are calculated from the fuzzy logic based on the phase plane analysis. At the same time, the maximum achievable braking forces are calculated according to the tire/road conditions. Then, the optimal nonlinear algorithm is proposed to distribute the tire braking forces. After that, the desired wheel slip of each tire obtained by using the inverse braking force model is tracked by the wheel slip controller. Finally, the corrective front steer angle and the braking torque of each tire are imported to the vehicle model. A validated 8-DOF model [19] and also a more complex model in CarSim are employed as vehicle model for simulation studies. The 8-DOF vehicle model includes the four motions of vehicle body as well as the rotational dynamics of the four wheels. The CarSim model is a more complex model considering suspension effects on vehicle dynamics and tire forces too.

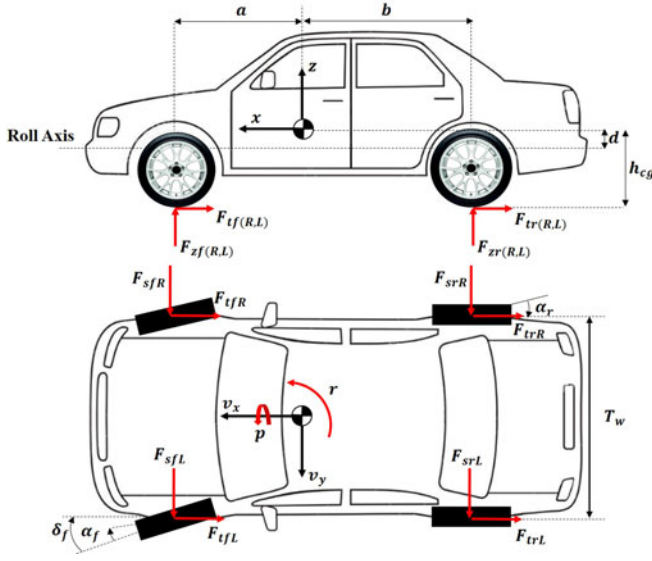


Fig. 2. 8-DOF vehicle model.

### III. CONTROL SYSTEM DESIGN

#### A. Integrated Controller Design

A multivariable nonlinear controller is optimally designed for the integrated AFS and DYC systems based on the 8-DOF model shown in Fig. 2. In this model, the four motions of vehicle body including the longitudinal velocity  $v_x$  the lateral velocity  $v_y$  the yaw rate  $r$ , and the roll rate  $p$  are employed for the integrated controller design with the following equations:

$$\dot{v}_x = \frac{1}{m} [m v_y r - F_{t_{fR}} - F_{t_{fL}} - F_{t_{rR}} - F_{t_{rL}}] \quad (1)$$

$$\dot{v}_y = \frac{1}{m} [-m v_x r + F_{s_{fR}} + F_{s_{fL}} + F_{s_{rR}} + F_{s_{rL}}] + \frac{1}{m} \Delta Y_{fc} \quad (2)$$

$$\dot{r} = \frac{1}{I_{zz}} [a(F_{s_{fR}} + F_{s_{fL}}) - b(F_{s_{rR}} + F_{s_{rL}})] + \frac{a}{I_{zz}} \Delta Y_{fc} + \frac{1}{I_{zz}} M_z \quad (3)$$

$$\dot{p} = \frac{1}{I_{xx}} [-m_s d \dot{v}_y - m_s d v_x r + m_s g d \sin(\phi_s) - K_\phi \phi_s - C_\phi p] \quad (4)$$

where,  $m$  and  $m_s$  denote the vehicle total mass and sprung mass, respectively.  $I_{zz}$  and  $I_{xx}$  are the yaw and roll moments of inertia,  $a$  and  $b$  are the distances of the mass center to the front and rear axles,  $d$  is the distance from the sprung mass to the roll axis,  $\phi_s$  is the roll angle, and  $K_\phi$  and  $C_\phi$  are the roll stiffness and damping coefficients.  $F_t$  and  $F_s$  are the longitudinal and lateral forces of tires, respectively, which are taken in directions of vehicle axes for small values of the front steering angle. Also, the corrective lateral force of the front wheels  $\Delta Y_{fc}$  and the required external yaw moment  $M_z$  are the two control inputs, which are determined from the integrated control law. Note that the product of inertia with respect to the roll and yaw axes is

taken to be zero [19]. Also, the coupling effect of roll motion and center of mass movement on the lateral acceleration is ignored for simplicity. The nonlinear Dugoff tire model that is based on the friction ellipse idea and includes the saturation property is selected to model the tire forces [19]. In this model, the relation for the longitudinal and lateral force of each tire is as follows:

$$F_t = \frac{C_\lambda \lambda}{1 - \lambda} f(s), \quad F_s = \frac{C_\alpha \tan(\alpha)}{1 - \lambda} f(s)$$

$$f(s) = \begin{cases} s(2-s), & s < 1 \\ 1, & s \geq 1 \end{cases}$$

$$s = \frac{\mu F_z (1 - \varepsilon_r v_x \sqrt{\lambda^2 + \tan^2(\alpha)})}{2 \sqrt{C_\lambda^2 \lambda^2 + C_\alpha^2 \tan^2(\alpha)}} (1 - \lambda). \quad (5)$$

For the Dugoff model,  $C_\lambda$  and  $C_\alpha$  are the longitudinal and cornering stiffness of the tire, respectively,  $\mu$  is the road coefficient of friction,  $\varepsilon_r$  is the road adhesion reduction factor,  $\lambda$  and  $\alpha$  are the longitudinal slip and the lateral slip angle of the tire, respectively. Also,  $F_z$  is the tire normal load of each tire. The normal loads of the front and rear tires including the dynamical load transfers due to the lateral and longitudinal accelerations and roll angle are expressed as follows:

$$F_{zf} = \frac{mg}{2} \left[ \frac{b}{l} - \frac{(\dot{v}_x - v_y r) h_{cg}}{g l} \pm K_{RSF} \left( \frac{h_{cg} a_y}{T_w g} - \frac{m_s d}{m T_w} \sin \phi_s \right) \right]$$

$$F_{zr} = \frac{mg}{2} \left[ \frac{a}{l} + \frac{(\dot{v}_x - v_y r) h_{cg}}{g l} \pm (1 - K_{RSF}) \left( \frac{h_{cg} a_y}{T_w g} - \frac{m_s d}{m T_w} \sin \phi_s \right) \right]. \quad (6)$$

In the above relations, the left and right tires are distinguished by, respectively, the positive and negative signs of the last term within the bracket. Also,  $a_y$  is the vehicle lateral acceleration,  $h_{cg}$  is the height of the vehicle center of gravity,  $K_{RSF}$  is the ratio of front roll stiffness to the total stiffness,  $l$  is the longitudinal wheel base, and  $T_w$  is the vehicle track width.

By defining the slip angle of the front and rear tires as  $\alpha_f = \delta_f - \tan^{-1} \left( \frac{v_y + ar}{v_x} \right)$  and  $\alpha_r = \tan^{-1} \left( \frac{br - v_y}{v_x} \right)$ , the state space form of (1) and (4) can be written as

$$\dot{x}_1 = g_1(\mathbf{x}, \delta_f) \quad (7)$$

$$\dot{x}_2 = g_2(\mathbf{x}, \delta_f) + \frac{1}{m} u_1 \quad (8)$$

$$\dot{x}_3 = g_3(\mathbf{x}, \delta_f) + \frac{a}{I_{zz}} u_1 + \frac{1}{I_{zz}} u_2 \quad (9)$$

$$\dot{x}_4 = g_4(\mathbf{x}, \delta_f) - \frac{m_s d}{m I_{xx}} u_1 \quad (10)$$

$$y = x_3 \quad (11)$$

in which  $\mathbf{x} = [x_1, x_2, x_3, x_4]^T = [v_x, v_y, r, p]^T$  is the state vector.  $\mathbf{u} = [u_1, u_2]^T = [\Delta Y_{fc}, M_z]^T$  represents the control inputs vector and  $y$  is the output.  $\delta_f$  is the front wheel steering

angle. The functions  $g_1, g_2, g_3$ , and  $g_4$  include the nonlinear Dugoff model (5).

Based on the vehicle state space model, a multivariable nonlinear controller is optimally developed using a predictive method to maintain the vehicle yaw rate close to its desired response. Concisely, the nonlinear yaw rate response for the next interval  $x_3(t+h)$  is first predicted by Taylor series expansion. Then, the current control signals will be found using a continuous minimization of the predicted tracking error. A quadratic pointwise performance index that penalizes both the next yaw rate tracking error and the current control signals is considered as follows [20], [21]

$$J_1[u_1, u_2] = \frac{1}{2}w_r[x_3(t+h) - x_{3d}(t+h)]^2 + \frac{1}{2}w_d u_1^2(t) + \frac{1}{2}w_m u_2^2(t) \quad (12)$$

where,  $w_r$ ,  $w_d$ , and  $w_m$  are the weight factors indicating the relative importance of the corresponding terms. Also,  $h$  is the predictive horizon and  $x_{3d}$  is the desired value for the vehicle yaw rate which will be explained in the following section. Note that the expensive strategy is employed here in which the weighted terms of the control inputs are included in the performance index (12) to be minimized. The optimum usage of each control input in different conditions is obtained by the regulation of control weights. The regulation policy will be discussed in the next sections with more details.

In order to develop the predicted response in terms of current control inputs,  $x_3(t+h)$  is expanded by a  $q$ th-order Taylor series at  $t$  as follows:

$$x_3(t+h) = x_3(t) + h\dot{x}_3(t) + \frac{h^2}{2!}\ddot{x}_3(t) + \dots + \frac{h^q}{q!}x_3^{(q)}(t). \quad (13)$$

The expansion order  $q$  is determined by the control order plus the relative degree of the nonlinear system [20], [22]. According to the system model, the output has the well-defined relative degree  $\rho = 1$ , which is determined as the lowest order of the derivative of the output in which the input first appears explicitly [23]. Moreover, for our system, the control order is selected to be zero so that the control effort will be a constant in the prediction interval. This selection, i.e., zero control order, leads to small control efforts and obtains relatively adequate performance for nonlinear systems with lower relative degree less than four [22]. It should be noted that when the control input is adopted to be a constant in the predictive interval, it is preferred to minimize a pointwise performance index with no integral to derive the optimal control laws in the closed forms. In this case, considering the performance index with integral leads to the control law with the same performance and only the values of free parameters including the weight factors and the prediction time are changed.

With the above reasoning, it is sufficient to expand the yaw rate and its desired value by the first-order Taylor series as

follows:

$$x_3(t+h) = x_3(t) + h\left(g_3 + \frac{a}{I_{zz}}u_1 + \frac{1}{I_{zz}}u_2\right) \quad (14)$$

$$x_{3d}(t+h) = x_{3d}(t) + h\dot{x}_{3d}(t). \quad (15)$$

Equations (14) and (15) are substituted into (12) to obtain the expanded performance index as a function of control inputs  $\Delta Y_{fc}$  and  $M_z$ . Finally, the control laws are obtained by applying the optimality conditions as follows:

$$\frac{\partial J_1}{\partial u_1} = 0 \Rightarrow A_{11}u_1 + A_{12}u_2 + B_1 = 0 \quad (16)$$

$$\frac{\partial J_1}{\partial u_2} = 0 \Rightarrow A_{21}u_1 + A_{22}u_2 + B_2 = 0. \quad (17)$$

Since the performance index has a quadratic form with respect to control inputs and the weight factors are considered positive values, the shape of function  $J_1$  is an elliptic paraboloid. So, it has a single minimum point. Therefore, the necessary conditions of (16) and (17) will be also sufficient for global optimality at each instant. By solving (16) and (17), the optimal control laws in the closed forms are derived as

$$u_1 = -\frac{1}{A_{11}}(A_{12}u_2 + B_1) \quad (18)$$

$$u_2 = \frac{B_2A_{11} - B_1A_{12}}{A_{12}^2 - A_{11}A_{22}} \quad (19)$$

where

$$\begin{aligned} A_{12} &= aw_r\left(\frac{h}{I_{zz}}\right)^2, & A_{11} &= aA_{12}\left(1 + \frac{w_d}{aA_{12}}\right) \\ B_1 &= A_{12}\left(\frac{I_{zz}}{h}\right)[e_r + h(g_3 - \dot{x}_{3d})], & A_{21} &= A_{12} \\ A_{22} &= \frac{A_{12}}{a}\left(1 + \frac{aw_m}{A_{12}}\right), & B_2 &= \frac{B_1}{a} \end{aligned} \quad (20)$$

and  $e_r$  is the current yaw rate tracking error defined as

$$e_r(t) = r(t) - r_d(t). \quad (21)$$

The expanded forms of the control laws of (18) and (19) can be also obtained by substituting the relations of (20) into (18) and (19) with some algebraic operations as

$$u_2 = -\frac{I_{zz}}{h} \frac{1}{1 + a^2 \frac{w_m}{w_d} + \frac{w_m}{w_r} \left(\frac{I_{zz}}{h}\right)^2} [e_r + h(g_3 - \dot{r}_d)] \quad (22)$$

$$u_1 = -\frac{I_{zz}}{h} \frac{1}{a + \frac{w_d}{aw_r} \left(\frac{I_{zz}}{h}\right)^2} \left(u_2 + \frac{I_{zz}}{h} [e_r + h(g_3 - \dot{r}_d)]\right). \quad (23)$$

The effective contribution of each control input can be assigned by a suitable regulation of the weight factors  $w_m$  and  $w_d$  with respect to  $w_r$ , which will be explained in Section III-C.

The error dynamics of yaw rate can be derived by applying the control law (18) and (19), which is based on the nominal

model, in the actual model (8) and (9). This operation together with some other algebraic operations leads

$$\dot{r} = g_3 - \frac{\kappa}{h}[e_r + h(\hat{g}_3 - \dot{r}_d)] \quad (24)$$

where

$$\kappa = \frac{1 + \frac{w_d}{a^2 w_r} \left(\frac{I_{zz}}{h}\right)^2 + a^2 \frac{w_m}{w_d} + \frac{w_m}{w_r} \left(\frac{I_{zz}}{h}\right)^2}{\left(1 + \frac{w_d}{a^2 w_r} \left(\frac{I_{zz}}{h}\right)^2\right) \left(1 + a^2 \frac{w_m}{w_d} + \frac{w_m}{w_r} \left(\frac{I_{zz}}{h}\right)^2\right)}. \quad (25)$$

Note that the symbol  $\hat{\cdot}$  denotes the nominal model employed in the control laws. The tracking error dynamics of yaw rate is obtained by rewriting (24) as follows:

$$\dot{e}_r + \frac{\kappa}{h} e_r = (g_3 - \hat{g}_3) + (1 - \kappa)(\hat{g}_3 - \dot{r}_d). \quad (26)$$

Deviation of  $g_3$  from the nominal model  $\hat{g}_3$  can be as a result of modeling uncertainties and also some possible errors in measurements and estimations. The function of  $\hat{g}_3$  is proportional to the internal yaw moment generated by the saturated tire lateral force and consequently is bounded. Therefore, the constants  $G > 0$  and  $\eta > 0$  can be considered such that

$$|g_3 - \hat{g}_3| \leq G, \quad |\hat{g}_3 - \dot{r}_d| \leq \eta. \quad (27)$$

Applying the bounds of (27) to the error dynamics (26) gives

$$\dot{e}_r + \frac{\kappa}{h} e_r \leq G + (1 - \kappa)\eta. \quad (28)$$

Solving the first-order differential equation with zero initial condition implies that the tracking error is bounded within

$$-e_m \leq e_r \leq e_m, \quad \text{for all } t \geq 0 \quad (29)$$

where

$$e_m = \frac{G}{\kappa} h + \frac{1 - \kappa}{\kappa} h \eta. \quad (30)$$

It is seen that the tracking error arises from both modeling uncertainties  $G$  and the control weight factors incorporated in  $\kappa$  according to (25).

In all analyses performed above, the constraints on control inputs are ignored. However, the physical limitation of control inputs will be considered in regulating the weight factors of control inputs and also in the distribution policy of tire forces.

### B. Desired Model for Vehicle Yaw Rate

In order to compensate the loss of vehicle directional stability caused by the saturation property of tire forces, a desired model of vehicle yaw rate is presented using the modified linear 2-DOF vehicle model. This model, developed in more details in [20] and [24], is expressed as follows:

$$\frac{r_d(s)}{\delta_f(s)} = G_R \frac{1}{1 + T_t s} \quad (31)$$

where

$$G_R = \frac{e_1 a_{21} - e_2 a_{11}}{a_{11} a_{22} - a_{12} a_{21}}, \quad e_1 = \frac{2C_{\alpha r}}{m v_x}, \quad e_2 = -\frac{2a C_{\alpha r}}{I_{zz}}$$

$$a_{11} = -2 \frac{C_{\alpha f} + C_{\alpha r}}{m v_x}, \quad a_{12} = 2 \frac{b C_{\alpha r} - a C_{\alpha f}}{m v_x^2} - 1$$

$$a_{21} = 2 \frac{b C_{\alpha r} - a C_{\alpha f}}{I_{zz}}, \quad a_{22} = -2 \frac{b^2 C_{\alpha r} + a^2 C_{\alpha f}}{I_{zz} v_x}.$$

In the above relations,  $r_d$  is the desired yaw rate which is tracked by the integrated controller and  $T_t$  is the time constant. To make the linear model response compatible with all driving conditions especially on slippery roads and during high speed maneuvers, the following limitation must be applied on the steady-state value of (31):

$$r_{ss} = \begin{cases} G_R \delta_f, & |G_R \delta_f| < \frac{\mu g}{v_x} \\ \frac{\mu g}{v_x} \text{sign}(G_R \delta_f), & \text{otherwise.} \end{cases} \quad (32)$$

As an important advantage, tracking the proposed desired model (31) which is limited by (32), leads to a significant reduction of the side slip angle. Therefore, an enhanced directional stability for vehicles through the limited yaw rate control is achieved.

### C. Fuzzy Logics for Regulation of the Weights

Fuzzy logics are defined for determination of the control weight factors  $w_d$  and  $w_m$  as the free parameters of the integrated control laws (22) and (23) with respect to  $w_r = 1$ . Regarding the integration policy of this study, the AFS and DYC are employed to track the desired yaw rate for improved steerability. In addition, the side slip angle,  $\beta \approx v_y/v_x$ , should be limited within admissible ranges to maintain the vehicle stability [25]. The activation and effective contribution of each control input to reach the desired responses in different conditions can be assigned by regulation of the control weight factors. The activation priority is given for AFS and the contribution of DYC increases when the AFS has no longer effect alone especially when the vehicle reaches the handling limit. In order to have a criterion for this purpose, the phase plane approach is employed. The stability bound obtained from the  $\beta - \dot{\beta}$  phase plane analysis of the nonlinear 2-DOF vehicle model for zero steer input is illustrated in Fig. 3. According to Fig. 3, while the initial conditions of the side slip angle and its rate lie close to origin, the trajectories converge to origin for a short time. The large side slip angle requires a long time for converging and is undesirable because of some physical limitation for the vehicle in the path. Therefore, a region is selected conservatively to observe the characteristics of vehicle stability.

The slope of the reference region boundaries is chosen to be the slope of the phase plane trajectories. The mathematics form of this region is formulated as

$$\left| \frac{1}{16} \dot{\beta} + \frac{1}{8} \beta \right| < 1. \quad (33)$$

It should be noted that the above region is conservatively defined to assure the vehicle stability in the presence of driver

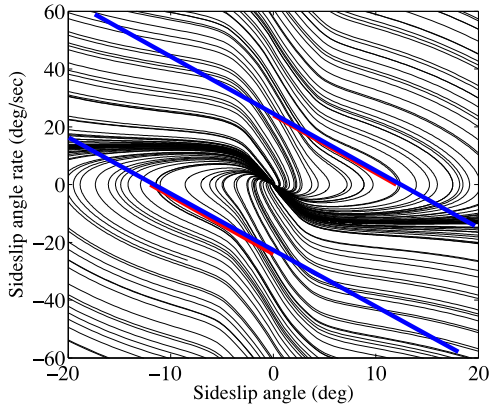


Fig. 3. Reference region based on the phase-plane analysis with zero steer input.

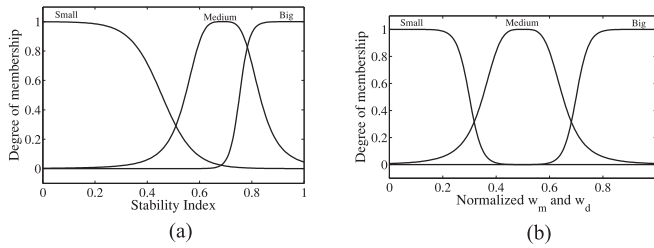


Fig. 4. Membership functions for (a) input variable and (b) output variable

TABLE I  
RULES OF FUZZY CONTROLLER

Stability index	$\hat{w}_d$
Small	Small
Medium	Medium
Big	Big

steer inputs. The relation (33) is referred to the stability index in the design of the member function for fuzzy logics.

Now, a fuzzy logic is developed to determine the control weight factors. The left term of relation (33) is considered as the input variable and the normalized weight  $\hat{w}_d$  is as the output variable of the fuzzy logic and the other normalized weight is calculated as  $\hat{w}_m = 1 - \hat{w}_d$ .

As shown in Fig. 4, three membership functions are defined and three linguistic variables are chosen for both input and output variables.

Table I shows the fuzzy rules for the proposed fuzzy logic. The rules are introduced on the basis of simple logics. For example, when the stability index is small, then  $w_d$  is needed to be small. This means that, the effective contribution of AFS is more than DYC in this condition.

The fuzzy logic uses the Mamdani fuzzy inference system, which is characterized by the following fuzzy rule schema: If stability index is A, then  $\hat{w}_d$  is B where A and B are fuzzy sets defined on the input and output domains. The defuzzification is performed using the center of area method. The universe of discourse of the output is normalized in the range [0, 1]. Finally, the fuzzy logic output  $\hat{w}_d$  is scaled to map the  $w_d$  from the

normalized interval as following:

$$w_d = (5 \times 10^{-13}) \hat{w}_d. \quad (34)$$

Also, after calculation of  $\hat{w}_m$  from  $\hat{w}_m = 1 - \hat{w}_d$ , it is scaled to map the  $\hat{w}_m$  as

$$w_m = (10^{-12}) \hat{w}_m. \quad (35)$$

The above scaling factors are adjusted by means of some trials. Note that the values of weight factors are set to very small numbers. However, in the implementation of the control laws (22) and (23), the ratio of weight factors and their multiplication by  $(I_{zz}/h)^2$  have been employed which are the normal numbers.

#### D. Design of Wheel Slip Controller

For the design of wheel slip controller, the longitudinal motion of the vehicle as well as the rotational dynamics of the four wheels are utilized as follows:

$$\dot{v}_x = -\frac{1}{m} \sum_{i=2}^5 F_{ti} \quad (36)$$

$$\dot{\omega}_i = \frac{1}{I_{wi}} [RF_{ti} - T_{bi}], \quad i = 2, 3, 4, 5 \quad (37)$$

where  $\omega$  is the angular velocity of wheel,  $I_w$  is the wheel moment of inertia, and  $R$  is the wheel radius. Also,  $F_i$  is the longitudinal tire force which is described by the Dugoff model (5) and  $T_b$  indicates the braking torque. The index  $i$  is defined as the number of each tire,  $2 = fL$ ,  $3 = rL$ ,  $4 = fR$ ,  $5 = rR$ .

By differentiating the longitudinal wheel slip during braking,  $\lambda_i = 1 - R\omega_i/v_x$ , with respect to the time and substituting (36) and (37) into the derivative form yields

$$\dot{\lambda}_i = -\frac{1}{v_x} \left[ \frac{1}{m} \left( \sum F_{ti} \right) (1 - \lambda_i) + \frac{R^2}{I_w} F_{ti} \right] + R \frac{T_{bi}}{I_w v_x}. \quad (38)$$

Therefore, the state space form of the nonlinear model described by (36) and (38), can be written as

$$\dot{x}_1 = f_1(\mathbf{x}) \quad (39)$$

$$\dot{x}_i = f_i(\mathbf{x}) + \frac{R}{I_w x_1} T_{bi} \quad (40)$$

$$\mathbf{y} = [x_2, x_3, x_4, x_5]^T \quad (41)$$

where  $\mathbf{x} = [x_1, x_2, x_3, x_4, x_5]^T = [v_x, \lambda_2, \lambda_3, \lambda_4, \lambda_5]^T$  is the state vector and  $\mathbf{y}$  is the outputs vector. The braking torques  $T_{bi}$  are considered as the control inputs. Also, the functions  $f_1$  and  $f_i$  include the nonlinear Dugoff tire model.

In order to develop the wheel slip control law, the prediction-based method of Section III-A is again applied. But, unlike the previous one, the cheap strategy [20] is employed here in which the control inputs  $T_{bi}$  are not penalized. Accordingly, a point-wise performance index minimizing the next instant tracking errors is defined as follows:

$$J_2[T_{bi}(t)] = \frac{1}{2} \sum_{i=2}^5 w_i [x_i(t+h_1) - x_{id}(t+h_1)]^2 \quad (42)$$

where,  $w_i$  are the weight factors for tracking errors of longitudinal slips and  $h_1$  is the predictive horizon. Index  $d$  denotes to the desired response.

Regarding the prediction-based control method, the nonlinear responses of the longitudinal slips of four wheels are first predicted by Taylor series expansion and then the performance index (42) can be obtained as a function of control inputs  $T_{bi}$ . Applying the optimality condition leads to

$$T_{bi} = -\frac{v_x I_w}{R h_1} [e_i + h_1 (f_i - \dot{\lambda}_{id})], \quad i = 2, 3, 4, 5 \quad (43)$$

where  $e_i$  is the current longitudinal slip tracking errors defined as

$$e_i(t) = \lambda_i(t) - \lambda_{id}(t), \quad i = 2, 3, 4, 5. \quad (44)$$

To achieve the maximum braking force during hard braking, the desired wheel slip for each tire  $\lambda_{id}$  can be instantaneously calculated by differentiating the longitudinal force described by the Dugoff tire model (5) with respect to the wheel slip as follows:

$$\left. \frac{\partial F_{ti}}{\partial \lambda_i} \right|_{\lambda_i = \lambda_{opt_i}} = 0. \quad (45)$$

By online solving the expanded form of (45), the optimum wheel slip  $\lambda_{opt_i}$  can be found [3]. Then, the maximum braking force  $F_{tmi}$  is calculated in this point through the Dugoff model (5) in terms of the tire normal load  $F_{zi}$  and the road friction coefficient  $\mu$  as  $F_{tmi} = F_{ti}(\lambda_{opt_i}, F_{zi}, \mu)$ . Note that the nonlinear Dugoff tire model is based on the friction ellipse idea and includes the saturation property of the tires. Therefore, the calculated maximum braking force is feasible and producible in practice.

In the conventional ABS, the optimum wheel slip calculated by (45) will be tracked to achieve the maximum braking force on various roads. However, in the hard braking during turning, the desired longitudinal slips should be calculated based on the proper braking force distribution. In such a way, by reducing the maximum achievable braking forces of one side wheels, the required external yaw moment is produced to maintain the vehicle in the path with a short stopping distance. Therefore, the desired longitudinal slip of each tire which will be tracked by the controller (43) is calculated from the corresponding force using an inverse braking force model. The inverse model is a piecewise linear model with high accuracy. In the following section, the longitudinal force distribution algorithm will be explained.

### E. Distribution Algorithm for Braking Forces

The final braking forces of tires  $F_{ti(i=2,\dots,5)}$  are distributed in a way that both short stopping distance and directional stability are provided. The distribution algorithm proposed here uses the maximum achievable braking forces  $F_{tmi(i=2,\dots,5)}$  and the external yaw moment  $M_z$  which is obtained from the control law (22).

When the braking forces of all wheels are at their maximum values, the yaw moment produced by the braking forces is

calculated as

$$M_{zm} = [(F_{tm4} + F_{tm5}) - (F_{tm2} + F_{tm3})] \frac{T_w}{2}. \quad (46)$$

Note that the difference between the maximum braking forces of the left and right wheels is as a result of longitudinal and lateral load transfers during braking and turning. By comparing  $M_{zm}$  and the required yaw moment  $M_z$  calculated from the control law (19) or (22), the following three cases can be occurred.

*Case 1:*  $M_{zm} = M_z$ . This case indicates  $F_{ti} = F_{tmi(i=2,\dots,5)}$  and is ideal for the hard braking during turning because the required stabilizing yaw moment is generated without any reduction in maximum braking forces. Therefore, the shortest stopping distance with improved directional stability is provided for the vehicle.

*Case 2:*  $M_{zm} < M_z$ . In this case, the forces of one side wheels must be kept at their maximum values and the forces from other side are reduced to compensate the required yaw moment. So, the following equation is used to find the reduced forces:

$$M_z = [(F_{tm4} + F_{tm5}) - (F_{t2} + F_{t3})] \frac{T_w}{2} \quad (47)$$

where  $M_z$  is obtained from (19) or (22). The above equation is solved for  $F_{t2}$  and  $F_{t3}$  with the following stages: First, the front tire force  $F_{t2}$  is set to its maximum value ( $F_{t2} = F_{tm2}$ ) and the reduced force of  $F_{t3}$  is found from (47). If more reduction is required,  $F_{t3}$  is set to zero and  $F_{t2}$  is found from (47) to be reduced. The load transfer due to braking causes the force capacity of the front tire to be more than that of the rear tire. This is the reason for the selection of the front tire force  $F_{t3}$  to be reduced at the first stage. Note that the maximum yaw moment generated by differential braking is obtained by getting the  $F_{t2}$  and  $F_{t3}$  to zero and  $F_{t4}$  and  $F_{t5}$  to their maximum values.

*Case 3:*  $M_{zm} > M_z$ . For this case, the strategy of case 2 is considered again by changing the place of left and right wheels.

As mentioned before, the maximum braking force of each tire is calculated by the nonlinear Dugoff model and is achievable in practice. Consequently, the final braking force of each tire which is a reduced value of the maximum braking force will be achievable in practice. Therefore, the following constraint indicating the tire work load will be always satisfied for the braked wheel

$$\frac{F_{si}^2 + F_{ti}^2}{(\mu F_{zi})^2} \leq 1, \quad i = 2, 3, 4, 5. \quad (48)$$

The left hand side of (48) is called the normalized work load.

## IV. SIMULATION RESULTS

The hard braking of vehicle with the initial speed of 90 km/h is first simulated during a turning maneuver in which the wheel steering angle is set at 5° after 1 s. The parameters of 8-DOF vehicle model are described in Table II.

It is assumed that the road friction coefficient is  $\mu = 0.8$ . In order to investigate the effect of structured uncertainties on the robust performance of the control system, some arbitrary uncertainties in the vehicle parameters can be considered. Here, the parametric uncertainties include +15% in the total mass,

TABLE II  
PARAMETERS OF THE CASE STUDY VEHICLES [19]

Parameter	Value	Parameter	Value
$m$	1280 kg	$R$	0.3 m
$m_s$	1160 kg	$I_w$	2.1 kg m <sup>2</sup>
$I_{zz}$	2500 kg·m <sup>2</sup>	$C_\alpha$	30000 N/rad
$I_{xx}$	750 kg·m <sup>2</sup>	$C_\lambda$	50000 N/unit slip
$a$	1.203 m	$\varepsilon_r$	0.015
$b$	1.217 m	$T_w$	1.33 m
$l$	2.42 m	$K_{RSF}$	0.444
$h_{cg}$	0.5 m	$K_\phi$	45000 N·m/rad
$d$	0.2 m	$C_\phi$	2600 N·m·s/rad

+5% in the road friction coefficient, +15% in the moment of inertia, and -20% in the tire stiffness. Also, a Gaussian white noise is added to the longitudinal wheel slip of tires which should be estimated in practice.

Different control strategies including stand-alone steering control, stand-alone braking control, and integrated braking and steering control are examined to control the vehicle in the mentioned maneuver. For all strategies, the prediction time is taken to be  $h = 0.05$  s. In the stand-alone steering control strategy, only the AFS control is employed to control the steered vehicle. In this case, it is assumed that the driver suddenly applies a hard braking to the vehicle for stopping and there is no control on braking system. The second strategy, stand-alone braking control, is a special case of the integrated control system in which the steering control is inactive, i.e.,  $w_d = \infty$  and the external yaw moment is fully used, i.e.,  $w_m = 0$ . However, in the integrated control strategy, the steering control will be integrated with the braking control to decrease the contribution of the external yaw moment while tracking the desired yaw rate, precisely. In what follows, the obtained results of three strategies will be compared. At first, the results are extracted using the 8-DOF vehicle model. Then, a more complex model in CarSim is employed as the vehicle model for the numerical simulation.

The yaw rate and side slip angle responses along with the control inputs obtained by three control strategies are shown in Fig. 5. As it is seen, the vehicle responses are unstable under stand-alone steering control. This is for the reason that all tires become locked under hard braking according to Fig. 6 and, therefore, the sensitivity of steering control on vehicle responses is lost.

In contrast, the reference model of the yaw rate is closely tracked by both the braking and the integrated controllers [see Fig. 5(a)]. In these cases, the vehicle side slip angle is limited and the longitudinal slips are controlled to prevent the tires from being locked (see Fig. 6). As a result, both control strategies improve the vehicle steerability and stability. However, as shown in Fig. 5(c), the contribution of external yaw moment in the integrated strategy is remarkably decreased. Since this moment is generated by reducing the maximum braking force of one side wheels, the vehicle stopping distance may be decreased in the integrated control. According to Table III, the stopping distance is decreased about 2.2 m by the integrated control in comparison with the stand-alone braking control. This

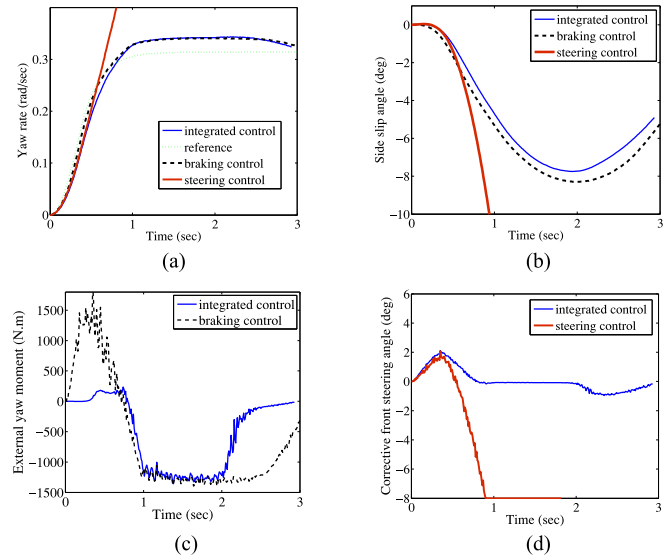


Fig. 5. Comparison of the vehicle responses and control inputs for different strategies: (a) yaw rate; (b) side slip angle; (c) external yaw moment; and (d) corrective front steering angle.

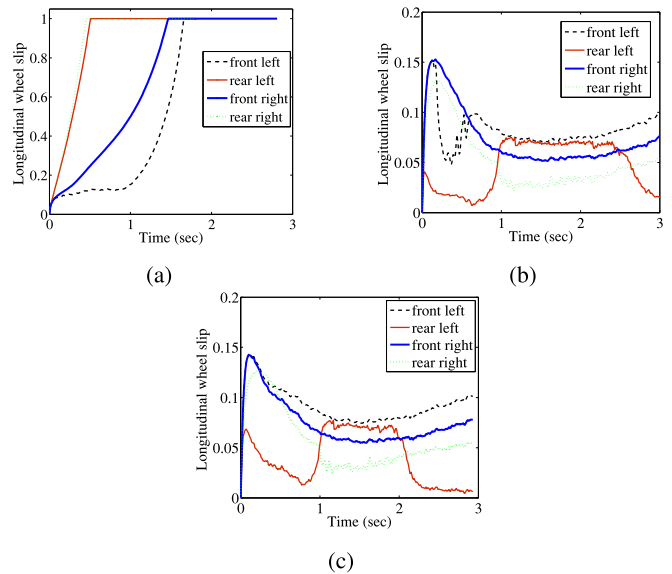


Fig. 6. Comparison of the longitudinal wheel slips: (a) steering control; (b) braking control; and (c) integrated control

TABLE III  
STOPPING DISTANCE FOR DIFFERENT CONTROL STRATEGIES

	8-DOF model	CarSim model
Braking control (m)	53.54	56.10
Integrated control (m)	51.35	53.14

reduction will be more when a more complex model in CarSim is employed as the vehicle model.

Here, the optimal integration of the steering and braking control is the reason of significant reduction of the required yaw moment. Therefore, the less reduction in the maximum braking forces is required for the integrated strategy which leads to the shorter stopping distance. Attention is called to the fact that in



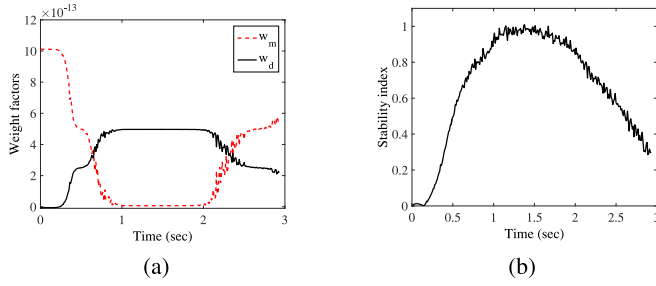


Fig. 7. Weight factors and the stability index for integrated control strategy.

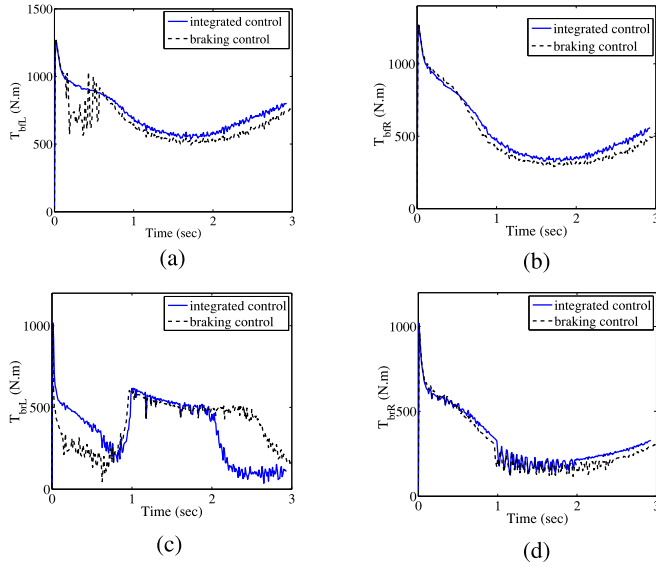


Fig. 8. Braking torques of (a) front left tire, (b) front right tire, (c) rear left tire, and (d) rear right tire.

braking control strategy the external yaw moment could be decreased by increasing its weight factor,  $w_m$ . But, this leads to the increased tracking error of yaw rate.

The control weight factors ( $w_m$  and  $w_d$ ) determined from the fuzzy logic are depicted in Fig. 7(a). It is considered that the weight factors are changing softly using the proposed fuzzy scheduled method. The decrease or increase of the weight factors shows the importance of control inputs relative to each other. Fig. 7(b) illustrates the stability index for different control strategies. When the stability index increases, the weights of the external yaw moment ( $w_m$ ) and the corrective lateral forces of the front wheels ( $w_d$ ) are decreased and increased, respectively, and vice versa.

After calculating the external yaw moment for both the braking and the integrated strategies, the braking forces are transversely distributed to generate the required moments. Finally, to produce the distributed braking forces, the braking torques applied to the wheels are calculated by the wheel slip controllers. Fig. 8 shows the braking torques of four wheels. The normalized work load of tires is depicted in Fig. 9. It can be seen that the normalized work load of all tires are below one. As a result, the calculated braking forces can be physically produced in practice according to (48).

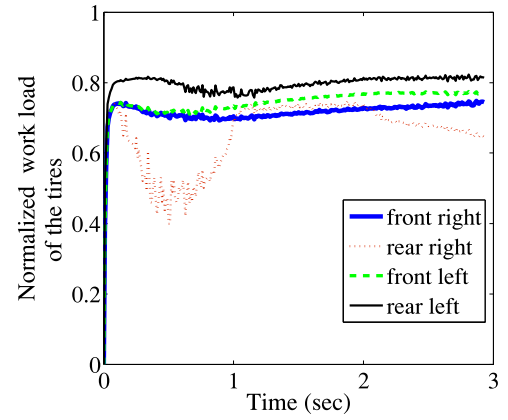


Fig. 9. Normalized work load of tires for the integrated control system.

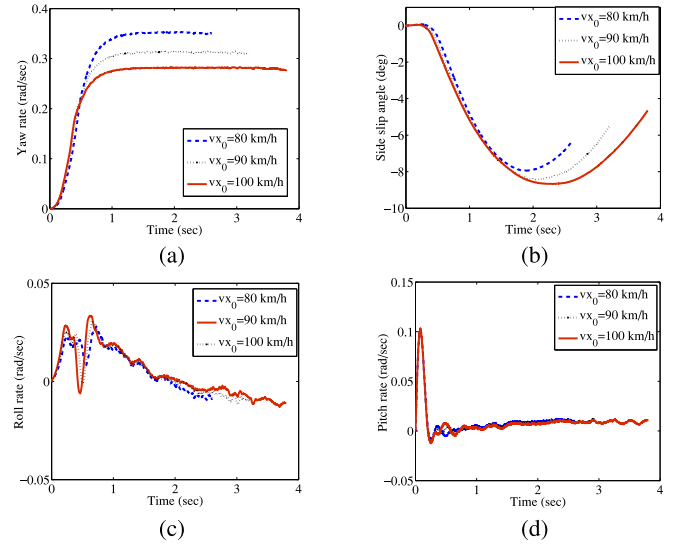


Fig. 10. The vehicle responses for the integrated control with different initial speeds using CarSim: (a) yaw rate; (b) side slip angle; (c) roll rate; and (d) pitch rate.

At the end of simulation studies, the overall performance of the developed control system at different driving conditions is presented using a more complex model in CarSim. The CarSim vehicle model takes into account pitch motion and suspension effects on vehicle dynamics and tire forces too. Therefore, the effects of uncertainties due to unmodeled dynamics can be investigated on the control system performance.

The former maneuver is considered again for different values of vehicle initial speeds and a constant value of road friction. Fig. 10 shows that the yaw rate responses of the vehicle with the integrated controller follow their own desired values. Also, the limited values of side slip angle indicate the stable behavior for the controlled vehicle. The responses of roll and pitch rate are illustrated in Fig. 10. The control weight factors obtained by the fuzzy logic and the stability index for three initial speeds are depicted in Fig. 11.

In another evaluation of the overall performance of the integrated control system using the CarSim vehicle model, a constant initial speed is considered for different friction coefficients. The stopping distance for all cases above are reported in Table IV and compared with those obtained by the stand-alone braking

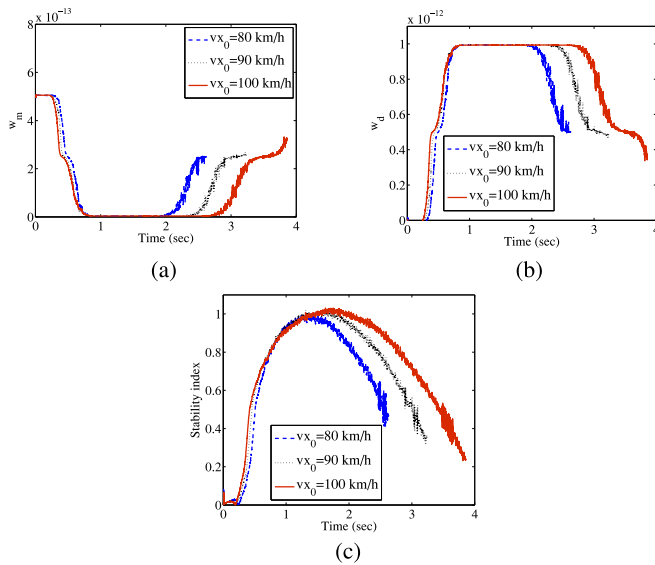


Fig. 11. Weight factors and the stability index of the integrated control with different initial speeds using CarSim.

TABLE IV

COMPARISON OF STOPPING DISTANCE FOR TWO CONTROL SYSTEMS WITH DIFFERENT CONDITIONS USING CARSIM MODEL

Conditions		Integrated control system (m)	Braking control system (m)
$\mu = 0.8$	$v_{x0} = 100$ km/h	68.53	71.73
	$v_{x0} = 90$ km/h	53.14	56.10
	$v_{x0} = 80$ km/h	39.52	42.26
$v_{x0} = 90$ km/h	$\mu = 0.8$	53.14	56.10
	$\mu = 0.6$	68.77	71.85
	$\mu = 0.4$	101.59	104.61

system. The results show a good performance of the proposed control system in facing to different conditions.

## V. CONCLUSION

To achieve the safe braking during turning, an integrated control system for vehicle braking and steering control has been optimally designed. The control laws in different layers of the system have been developed based on the prediction of nonlinear vehicle responses. Using the stability index obtained by the phase plane analysis, fuzzy logics have been defined to determine the weights of each control input in various conditions. The simulation results demonstrate that the proposed integrated control system leads to the improved directional stability. Also, it achieves the shorter stopping distance in comparison with stand-alone braking control system.

## REFERENCES

- [1] Y. Oniz, E. Kayacan, and O. Kaynak, "A dynamic method to forecast the wheel slip for antilock braking system and its experimental evaluation," *IEEE Trans. Syst., Man, Cybern., B, Cybern.*, vol. 39, no. 2, pp. 551–560, Apr. 2009.
- [2] H. Mirzaeinejad and M. Mirzaei, "A novel method for non-linear control of wheel slip in anti-lock braking systems," *Control Eng. Practice*, vol. 18, pp. 918–926, 2010.
- [3] H. Mirzaeinejad and M. Mirzaei, "A new approach for modelling and control of two-wheel anti-lock brake systems," *Proc. Inst. Mech. Eng., K, J. Multi-body Dyn.*, vol. 225, pp. 179–192, 2011.
- [4] E. Dincmen, B. A. Guvenc, and T. Acarman, "Extremum-seeking control of ABS braking in road vehicles with lateral force improvement," *IEEE Trans. Control Syst. Technol.*, vol. 22, no. 1, pp. 230–237, Jan. 2014.
- [5] H. Mirzaeinejad and M. Mirzaei, "Optimization of nonlinear control strategy for anti-lock braking system with improvement of vehicle directional stability on split-roads," *Transp. Res. C, Emerg. Technol.*, vol. 46, pp. 1–15, 2014.
- [6] K. Nam, H. Fujimoto, and Y. Hori, "Advanced motion control of electric vehicles based on robust lateral tire force control via active front steering," *IEEE/ASME Trans. Mechatronics*, vol. 19, no. 1, pp. 289–299, Feb. 2014.
- [7] M. Abe, "Vehicle dynamics and control for improving handling and active safety: from four-wheel steering to direct yaw moment control," *Proc. Inst. Mech. Eng., K, J. Multi-body Dyn.*, vol. 213, pp. 87–101, 1999.
- [8] D. Li, S. Du, and F. Yu, "Integrated vehicle chassis control based on direct yaw moment, active steering and active stabiliser," *Veh. Syst. Dyn.*, vol. 46, pp. 341–351, 2008.
- [9] A. Goodarzi and E. Esmailzadeh, "Design of a VDC system for all-wheel independent drive vehicles," *IEEE/ASME Trans. Mechatronics*, vol. 12, no. 6, pp. 632–639, Dec. 2007.
- [10] Ph. Heinzl, P. Lugner, and M. Plochl, "Stability control of passenger car by combined additional steering and unilateral braking," *Veh. Syst. Dyn.*, vol. 37, pp. 221–233, 2002.
- [11] X. Yang, Z. Wang, and W. Peng, "Coordinated control of AFS and DYC for vehicle handling and stability based on optimal guaranteed cost theory," *Veh. Syst. Dyn.*, vol. 47, pp. 57–79, 2009.
- [12] M. Boada, B. Boada, A. Munoz, and V. Diaz, "Integrated control of front-wheel steering and front braking forces on the basis of fuzzy logic," *Proc. Inst. Mech. Eng., D, J. Automobile Eng.*, vol. 220, pp. 253–267, 2006.
- [13] G. Burgio and P. Zegelaar, "Integrated vehicle control using steering and brakes," *Int. J. Control*, vol. 79, pp. 534–541, 2006.
- [14] T. Acarman, "Nonlinear optimal integrated vehicle control using individual braking torque and steering angle with on-line control allocation by using state-dependent Riccati equation technique," *Veh. Syst. Dyn.*, vol. 47, pp. 155–177, 2009.
- [15] J. Tjonas and T. A. Johansen, "Stabilization of automotive vehicles using active steering and adaptive brake control allocation," *IEEE Trans. Control Syst. Technol.*, vol. 18, no. 3, pp. 545–558, May 2010.
- [16] T. Hwang, K. Park, S. J. Heo, S. Lee, and J. Lee, "Design of integrated chassis control logics for AFS and ESP," *Int. J. Automotive Technol.*, vol. 9, pp. 17–27, 2008.
- [17] S. Di Cairano, H. E. Tseng, D. Bernardini, and A. Bemporad, "Vehicle yaw stability control by coordinated active front steering and differential braking in the tire sideslip angles domain," *IEEE Trans. Control Syst. Technol.*, vol. 21, no. 4, pp. 1236–1248, Jul. 2013.
- [18] L. Fortuna and G. Muscato, "A roll stabilization system for a monohull ship: Modeling, identification, and adaptive control," *IEEE Trans. Control Syst. Technol.*, vol. 4, no. 1, pp. 18–28, Jan. 1996.
- [19] D. E. Smith and J. M. Starkey, "Effects of model complexity on the performance of automated vehicle steering controllers: Model development, validation and comparison," *Veh. Syst. Dyn.*, vol. 24, pp. 163–181, 1995.
- [20] M. Mirzaei, G. Alizadeh, M. Eslamian, and S. Azadi, "An optimal approach to non-linear control of vehicle yaw dynamics," *Proc. Inst. Mech. Eng., I, J. Syst. Control Eng.*, vol. 222, pp. 217–229, 2008.
- [21] P. Lu, "Optimal predictive Control of continuous nonlinear system," *Int. J. Control*, vol. 62, pp. 633–649, 1995.
- [22] W. H. Chen, D. J. Ballance, and P. J. Gawthrop, "Optimal control of nonlinear systems: A predictive control approach," *Automatica*, vol. 39, pp. 633–641, 2003.
- [23] J. J. E. Slotine and W. Li, *Applied Nonlinear Control*, vol. 199. Englewood Cliffs, NJ, USA: Prentice-Hall, 1991.
- [24] M. Mirzaei, "A new strategy for minimum usage of external yaw moment in vehicle dynamic control system," *Transp. Res. C, Emerg. Technol.*, vol. 18, pp. 213–224, 2010.
- [25] J. He, "Integrated vehicle dynamics control using active steering, driveline and braking," Ph.D. dissertation, School Mech. Eng., Univ. Leeds, Leeds, U.K., 2005.



**Mehdi Mirzaei** received the B.Sc., M.Sc. and Ph.D. degrees in mechanical engineering from the University of Tabriz, Tabriz, Iran, in 1999, 2002, and 2008, respectively.

Since 2008, he has been with the Mechanical Engineering Department, Sahand University of Technology (SUT), Tabriz, where he is currently an Associate Professor. He is also the Director of the Research Laboratory of Mechatronics and Vibrations, SUT. His current research interests include optimal control of nonlinear systems, automotive control systems, active vibration control, and mechatronics.



**Hossein Mirzaeinejad** received the B.Sc. degree in mechanical engineering from the University of Sistan and Baluchestan, Zahedan, Iran, in 2006, and the M.Sc. and Ph.D. degrees in mechanical engineering from the Sahand University of Technology, Tabriz, Iran, in 2010 and 2015, respectively.

He is currently an Assistant Professor with the Department of Mechanical Engineering, Shahid Bahonar University of Kerman, Kerman, Iran. His current research interests include vehicle dynamics and automotive control systems, nonlinear control, and robotics.